Towards the Interpretation of Hudson's Experiment on the Belousov-Zhabotinsky Reaction

——*Chaos Due to Delocalization*——

Kazuhisa TOMITA and Ichiro TSUDA

Department of Physics, Kyoto University, Kyoto 606

With reference to the experimental findings (by Hudson et al.) on the chaotic behaviour of the Belousov-Zhabotinsky reaction, a new model is proposed in terms of Poincaré return maps. The model leads to a series of consecutive periodic and chaotic phases in the control parameter space, which resembles closely to the overall characteristics observed by Hudson et al. The experimental data are further shown to be consistent with the proposed idea through an additional simulation based on an empirical transfer function.

§ 1. Introduction

Recently the chaotic behaviour of the Belousov-Zhabotinsky reaction has been carefully re-examined by Hudson et al.[1] in a stirred flow condition. Their results consist of a remarkably regular cascades of transition between a series of modes of limit cycle, and associated with each step they found a narrow but reproducible range for chaotic behaviour. The experimental results are summarized in Table I and Fig. 1. For later convenience abbreviated mode notations are introduced in Table I, i.e., (1) $\pi(n)$: a n-peaked periodic mode, (ii) $\pi_{l_n, l_{n+1}}(n, n+1)$: a periodic switching between l_n times $\pi(n)$-like and l_{n+1} times $\pi(n+1)$-like modes, and (3) $\chi(n, n+1)$: a chaotic switch between $\pi(n)$-like and $\pi(n+1)$-like modes. Let us here point out a simple quantitative relation existing among the series of periodic modes observed, which may lead to an interpretation of the associated chaos. First of all the observed modes consist clearly of two different kinds of oscillations, namely one with a large amplitude $A(\sim 40\,\mathrm{mV})$ and a long period T and the other with a small amplitude $a(\sim 6\,\mathrm{mV})$ and a short period τ.[*] (cf. Fig. 1) Comparing the two extremes in parameter space it is found that $T \sim 2\tau$, where $\tau \sim 0.48$ min. In addition it is reported that on further increasing the rate of flow the smaller limit cycle continues into a stable steady state i.e., the flow-induced steady state. On the other hand, it is expected that on decreasing the rate of flow one should reach another stable steady state, i.e., the flowless bulk branch.

---

[*] It is admitted that the absolute value of the observed potential (in millivolts) is not changing in a monotonic way with the control parameter, for which the origin is unknown to the authors. Nonetheless, the amplitudes of oscillation are fairly uniform.[7]

It is interesting to note that these characteristics resemble closely to that obtained in our simulation using a simplified three-variable model.[2] There also appears a change from a large limit cycle into a small one on increasing the rate of flow and in between a chaotic behaviour was found. Furthermore the period of the large limit cycles was found approximately twice that of the small ones. The only difference lies in that instead of a single chaotic intermediate a cascade of them was found in the experiment. In this paper we are interested in the possible mechanisms which form the background of the above stated features.

Let us denote the period of p-peaked limit cycle by T_p, and then one finds a very simple rule which is obeyed by the consecutive limit cycles observed, namely

Fig. 1. Observed temporal characteristics of Br⁻ electrode potential in the Belousov-Zhabotinsky Reaction (cf. Ref. 1)).
(a) Rate of flow=4.34 ml/m—$\pi(3)$
(b) Rate of flow=4.51 ml/m—$\chi(3,4)$
(c) Rate of flow=4.61 ml/m—$\pi(4)$
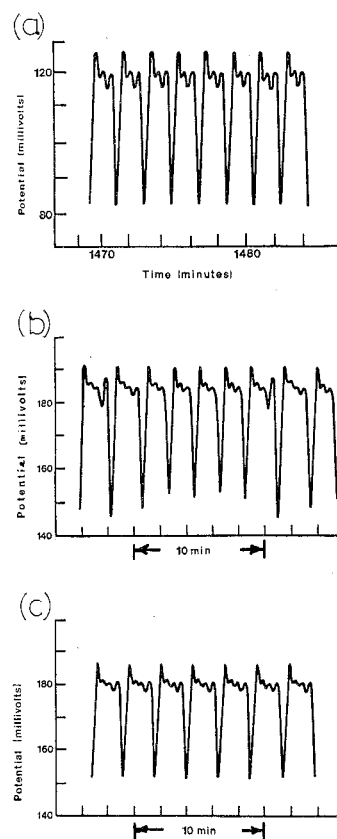See Table I for the corresponding descriptions.

Table I. The observed characteristics of the Belousov-Zhabotinsky reaction as a function of the rate of flow. For later convenience abbreviated mode notations are defined in this table. —— $\pi(n)$: a n-peaked periodic mode. $\pi_{l_n, l_{n+1}}(n, n+1)$: a periodic switching between l_n times $\pi(n)$-like and l_{n+1} times $\pi(n+1)$-like modes. $\chi(n, n+1)$: a chaotic switch between $\pi(n)$-like and $\pi(n+1)$-like modes.

	Rate of flow ml/m	Mode		Description
(a)	2.91	$\pi(1)$	——	1-peaked periodic mode
(b)	3.76 ⋯⋯	$\pi_{1,1}(1,2)$		periodic switching between 1- and 2-peak modes
(c)	4.06	$\pi(2)$	——	2-peaked periodic mode
(d)	4.31 ——	$\chi(2,3)$		chaotic switching between 2- and 3-peak modes
(e)	4.34	$\pi(3)$	——	3-peaked periodic mode
(f)	4.51 ——	$\chi(3,4)$		chaotic switching between 3- and 4-peak modes
(g)	4.62	$\pi(4)$	——	4-peaked periodic mode
(h)	4.76 ——	$\chi(4,5)$		chaotic switching between 4- and 5-peak modes
(i)	4.81	$\pi(5)$	——	5-peaked periodic mode
(j)	5.37	$\pi(m)$	——	multi peaked periodic mode
(k)	5.42	$\pi^*(1)$		1-peaked periodic mode (* small amplitude, short period)
(l)	>5.5	F		flow-induced steady state

Table II. Relation among periodic phases. The period T_p of p-peaked periodic modes is shown to obey a simple rule, i.e., Eq. (1).

$p\binom{\text{Number}}{\text{of peaks}}$	T_p (obs)	T_p (theor)	T_p (obs)-T_p (theor)	$\dfrac{T_p\,(\text{obs})\cdot T_p\,(\text{theor})}{T_p\,(\text{theor})}$
1	0.96 min	0.96 min	0.00 min	0.0%
2	1.34	1.44	−0.10	−6.9
3	1.88	1.92	−0.04	−2.1
4	2.58	2.40	0.10	4.1
5	2.88	2.88	0.00	0.0

period $T_p(\text{theor}) = T + (p-1)\tau$, $T = 2\tau$ ($\tau = 0.48$ min)

$$T_p = T + (p-1)\tau \simeq (p+1)\tau, \qquad (1)$$

where $\tau \sim 0.48$ min and $p = 1, 2, 3, 4$ and 5. The comparison between the observed and the predicted periods is surprisingly good as is shown in Table II. As the large amplitude mode has a very large excursion from the flow-induced branch to the direction of the bulk branch, it is natural to expect that the large amplitude mode encircles not only the flow-induced branch but also the bulk branch. From this point of view the relation $T \sim 2\tau$ suggests that both branches have periods of the same order of magnitude τ in their own basins, and that there exists a communication between the two basins across an intervening saddle in the relevant range of the control parameter. This means that the large amplitude mode observed corresponds to a delocalized orbit encircling both branches in contrast to the small amplitude mode which encircles the flow-induced branch only. And it is our contention that this kind of delocalization is closely related to the appearance of chaotic orbits. In other words an interplay between a soft-mode instability and a pair of hard-mode instabilities is closely related to the appearance of chaos. In Fig. 2 a typical example is shown, in which a soft-mode instability (A, A') is embraced by a pair of hard-mode instabilities (B) and (B'). Without the hard-mode instabilities the two branches of soft-mode instability have their own
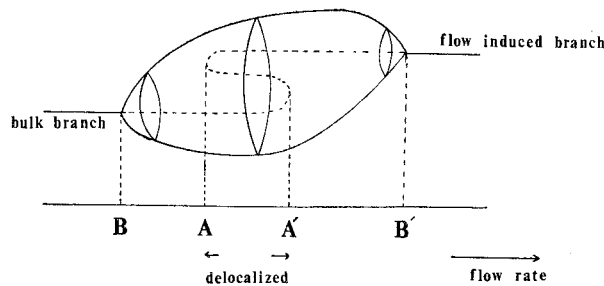

Fig. 2. Interplay of soft- and hard-mode instabilities. Phase coordinates of the steady states, represented as a single vertical dimension, are plotted against the control parameter (flow rate).

basins separated by an intervening saddle and represent a bistability. However, under the simultaneous appearance of the hard-mode instabilities on both sides all three steady states become unstable and there are no exact definitions of separate basins. The two solid lines between B and B′ indicate the two extremes of limit cycle orbits, which is delocalized to encircle the two branches at least in the middle part (A, A′). It is our contention that at least in this range the orbit is bound to be delocalized and may lead to a chaotic behaviour. In the following sections the possibility of chaos due to this kind of delocalization will be discussed by starting with the general classification of the communication of two basins across an intervening saddle in three dimensional space.

§ 2. Communication of two basins across a saddle

——*A piece-wise linear model leading to chaos*——

Let us confine ourselves to the case of three dimension (x, y, z), and suppose the existence of a two dimensional separatrix crossing a saddle at the origin (O), which is defined by the stable manifold $W^s(O)$ of this point. The unstable manifold $W^u(O)$ may either be confined within a finite distance from O or be tending to infinity. In the latter case the stable manifold is required to have complex eigenvalues at O in order for a delocalized orbit to appear. Let us, however, suppose for the moment the former case and also that $W^s(O)$ has two real eigenvalues at O. Suppose that the z-axis belongs to $W^s(O)$ and let us look at the projection onto the $(x-y)$ plane. The intersection of this plane with $W^s(O)$ may be split into two branches $W_i^s(O)$ $(i=1, 2)$ starting from O. Suppose the fixed point i is closer to $W_i^s(O)$ as is shown in Fig. 3, then they define basin i, i.e. the upper (1) and the lower (2) basins indicated in Table III, at least locally, and one is here interested in the communication between these two basins, i.e., delocalization of the orbit. Then, according to the relation between $W^s(O)$ and $W^u(O)$ there appear the following three cases.
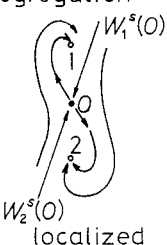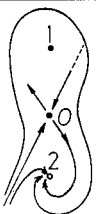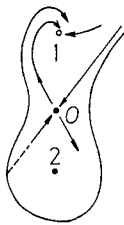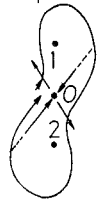Case A:
The separatrix $W^s(O)$ is global in character. In other words it extends to infinity. In this case the two basins are completely separated, each having its own asymptotic state. This may be called the case of segregation.
Case B:
The separatrix $W^s(O)$ is global in only one of the two directions in the projection. In other words $W_1^s(O)$ extends to infinity, whereas $W_2^s(O)$ stands local (or vice versa). In this case there is only one asymptotic state as is clear from Table III. However, in the transient situation there may be two kinds of orbits which are markedly different in character in its relation to $W_1^s(O)$. The non-trivial species corresponds in general to a giant transitory excitation,[3] therefore this case may be characterized by the excitability.

Table III. Communication of two basins across an intervening saddle. The phase portraits are indicated in 2-dimensional projections in the figures. The focus in upper (lower) basin is indicated by 1(2). The overall situation is classified according to the ranges of influence of the two branches of separatrix $W_1^s(O)$ and $W_2^s(O)$, i.e., whether the influence is global or local. Delocalization appears when both $W_1^s(O)$ and $W_2^s(O)$ are local in their influence.

Case C:

The separatrix $W^s(O)$ is local in character in every direction. In this case no localization is assured in one of the two apparent basins, and various modes of delocalization are expected according to the values of the control parameter in the system. In addition to the periodic delocalization of one sort or another, chaotic delocalization, i.e., irregular communication of basins, may appear in this case. This situation is investigated in more detail in the remaining part of this paper under several simplifying assumptions.

Let us first consider an orbit which traces approximately n loops in the upper basin, then just a single loop in the lower basin, and finally comes back to the original basin to resume a new sequence similar to that which has been describ-ed.[*]

Suppose the change in the behaviour of the orbit is incurred mainly in the upper basin (the flow-induced branch) when the control parameter (the rate of

---

[*] This kind of behaviour is expected when an unstable limit cycle exists in each basin, the one in the lower basin having relatively large radius. However, it is not necessary to postulate such unstable limit cycles, and the corresponding wide-range flat tops of the potential will suffice.

flow) is changed, and there appears little corresponding change in the lower basin (the bulk branch), so that the situation is asymmetric with respect to the interchange of basins. In order to visualize the situation in a more quantitative way the Poincaré return maps are now invoked. Let us for this purpose take two planes $z = z_1$ and $z = z_2$ ($z_2 > z_1$, say), and indicate the upward crossing point of the orbit with the former and the downward crossing point with the latter as the Poincaré return maps. The simplest way to parametrize these sections is to use the angle spanned by the representative points at the origin O with reference to a particular direction, which, in this case, is chosen as the direction of the projected unstable manifold $W_1{}^u(O)$ in the upper basin. Let us parametrize the section with $z = z_1$ by the angle δ_k and that with $z = z_2$ by the angle θ_k, respectively, where k indicates the k-th reinjected orbit into the upper basin. In other words δ_k stands for the angular drift of the k-th arriving orbit and θ_k stands for that of the k-th departing orbit, respectively. In addition the anglar drift between $W_1{}^u(O)$ and $W_1{}^s(O)$ is indicated by Θ. Instead of θ_k, then, one may introduce a new quantity $\varepsilon_k \equiv \theta_k - \Theta$, i.e., the residual drift of the k-th departing orbit, which is used in the following. Finally let us define the angular drift D of the orbit
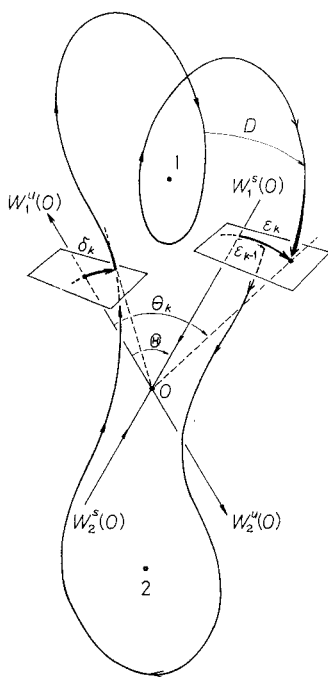

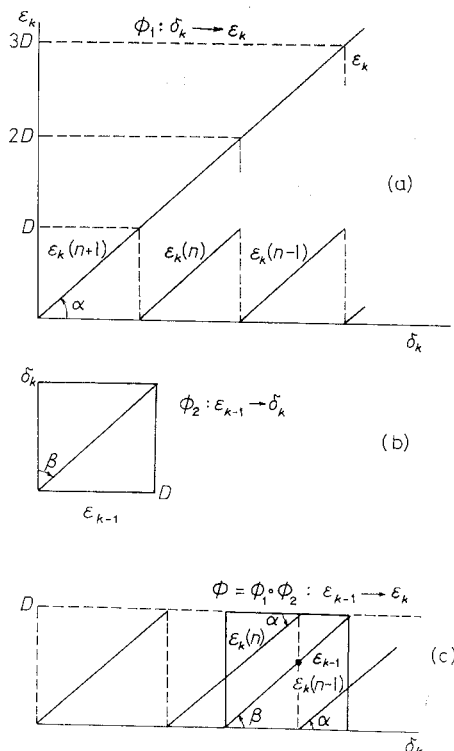Fig. 3. Phase portrait, definition and parametrization of Poincaré sections

Fig. 4. Lorenz plot (Poincaré return map of one dimension). (a) $\phi_1: \delta_k \to \varepsilon_k$, (b) $\phi_2: \varepsilon_{k-1} \to \delta_k$, (c) $\phi = \phi_1 \circ \phi_2: \varepsilon_{k-1} \to \varepsilon_k$

per cycle in the upper basin.

To describe the behaviour of the orbit on the sections defined above let us now introduce two discrete mappings, i.e., $\phi_1: \delta_k \to \varepsilon_k$ and $\phi_2: \varepsilon_{k-1} \to \delta_k$, and assume the following characteristics. On increasing δ_k, ε_k is expected to increase monotonically, however when ε_k reaches the value D the number of cycles traced by the orbit before leaving the upper basin is reduced by one and the new value of ε_k starts from zero again. This is indicated by the saw-tooth behaviour of ϕ_1 in Fig. 4(a).

On the other hand, the behaviour of the orbit in the lower basin is ruled by the simple monotonic transformation ϕ_2 indicated by Fig. 4(b), for it is assumed that the orbit traces only one cycle in the lower basin. For both mappings linear dependences are assumed in what follows which will be satisfactory in the discussion of the qualitative behaviour.

Let us now suppose that the global behaviour of the orbit is determined by combining two consecutive mappings ϕ_1 and ϕ_2. One is then lead to a resultant mapping $\phi: \varepsilon_{k-1} \to \varepsilon_k$ by eliminating δ_k through $\phi = \phi_1 \cdot \phi_2$, or one may plot both ε_{k-1} and ε_k against the same parameter δ_k. An example of such contracted plot is shown in Fig. 4(c). In the construction of $\phi((c))$ from $\phi_1((a))$ and $\phi_2((b))$ the only thing to be fixed is the relative position of the origins of ϕ_1 and ϕ_2. Noting that the change $\Delta\delta_k$ in δ_k is equivalent to $-\Delta\Theta$ in Θ, one may realize that the relative position of the origins of ϕ_1 and ϕ_2 is determined by the saddle angle Θ, which in turn is a function of the control parameter inherent in the system (e.g. the flow rate).

With the Poincaré return map ϕ in hand the situation for a fixed value of the control parameter may be classified according to the relation between the two angles α and β, which describe the characteristics of ϕ_1 and ϕ_2, respectively (cf. Figs. 4(a) and (b)).

Case I: $\alpha \lesssim \beta$

In this case there exists at most one peak of the saw-tooth in the whole interval, which may correspond to the abrupt change from $n+1 \to n$ cycles in the upper basin.

When there exists no peak in the whole interval, as shown in Figs. 5(a) and (c), there clearly appears one stable fixed point which corresponds to a periodic orbit which consists of either n or $n+1$ cycles in the upper basin continuing into a single cycle excursion in the lower basin. This is approximately the situation which was supposed earlier. This kind of periodic mode may be indicated by $\pi(n+1)$ or $\pi(n)$. In Fig. 5 the abscissa is taken as ε_{k-1} instead of δ_k in Fig. 4. Accordingly it is understood that $\beta = \pi/4$ hereafter.

When there exists a single peak in the whole interval, as shown in Fig. 5(b), there appears a switching between a $\pi(n)$-like and a $\pi(n+1)$-like modes. It is interesting to note that this switching itself may either be periodic or be aperiodic practically, according to the relative position of the origins of ϕ_1 and
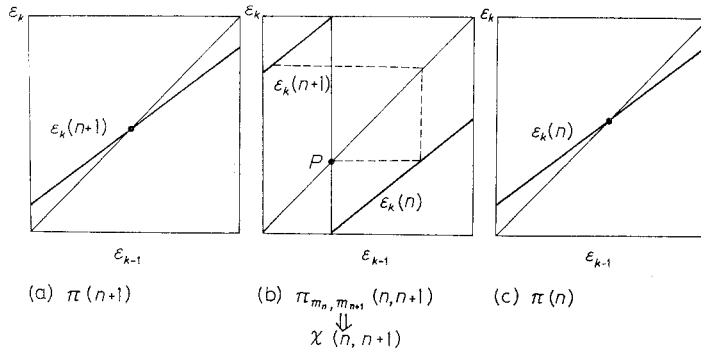
Fig. 5. Possible cases in the Lorenz plot. (a) $\pi(n+1):(n+1)$-peaked periodicity, (b) switching between $\pi(n)$-like and $\pi(n+1)$-like modes, (c) $\pi(n):n$-peaked periodicity.

ϕ_2. Resorting to the piecewise linear approximation to ϕ_1 and ϕ_2, one may explicitly write down the relevant conditions for specific results.

First it should be noted that the steep step in the shift map is an indication of its remarkable expanding property in the close neighbourhood of the saddle. The map, however, is weakly contracting everywhere in the remaining part of the interval, as $\alpha \lesssim \beta$. As a result a gap or a forbidden band is born at each step of mapping from the neighbourhood of the steep step, i.e., the saddle. The gaps thus generated would split the interval into pieces, provided no amalgamation of gaps appears. However, this is not the case at least for a purely stable linear map. This means that at some stage the gap overrides the saddle. From this stage on, amalgamations of gaps emerge and the increase is seen not in the number of gaps but in the size of the individual gaps. This then leads to a finite number of fixed points, which reflect the existence of a stable periodic orbit, however long its period may be.

To look into a little more details let us suppose that steep step is placed at a distance a from the lower of the interval, and the transfer function ϕ intersects $\varepsilon_k = \varepsilon_{k-1}$ at the point P. Without loss of generality one may assume a to be smaller than one-half of the interval. Suppose that, starting from P, one may reach the $\pi(n+1)$-like branch AB at the point Q after m-steps of inverse mapping with respect to the $\pi(n)$-like branch CD (see Fig. 6). The condition imposed on a in this case is found to be

$$\frac{\rho}{1+\rho+\cdots+\rho^{m+1}} < a^* < \frac{1}{1+\rho+\cdots+\rho^m}, \tag{2}$$

where

$$a^* \equiv a(\Theta)/D \cot \beta \tag{3}$$

and

$$\rho \equiv \tan\beta/\tan\alpha > 1 . \qquad (4)$$

It is easy to show that outside these intervals for all m there appear periodic motions. Let us therefore confine our attention inside this interval, and define two forward sequences of mapping starting from the upper and lower ends of the interval, respectively. As $\alpha < \beta$ these two maps define a gap or a forbidden band in the interval. One then asks at what stage of the mapping the image of the gap overrides the saddle (or the steep step) for the first time. Suppose the gap overrides the saddle for the first time at the n-th mapping the number of gaps cannot increase beyond n, which implies that there appears $(n+1)$ fixed points asymptotically.

Fig. 6. Analysis of switching process between $\pi(n)$-like and $\pi(n+1)$-like modes. (The case $m=1$ is indicated. cf. Fig. 5(b).) See the main text for the meaning of symbols.

An economic method is described in the Appendix for finding the condition under which the first overriding appears at the n-th stage of mapping.

The results of an elementary analysis are given as follows:
For the mode $\pi_{2m+1,2}$

$$\frac{(\rho-1)(\rho^{m+2}+1)}{\rho^{2m+3}-1} < \frac{a}{D} < \frac{\rho(\rho-1)(\rho^{m+1}+1)}{\rho^{2m+3}-1} . \qquad (5)$$

For the mode $\pi_{3m+1,3}$

$$\frac{\rho(\rho-1)(\rho^{3m+3}-1)-(\rho-1)^2(\rho^{m+1}-1)}{(\rho^{m+1}-1)(\rho^{3m+4}-1)} < \frac{a}{D} < \frac{\rho(\rho-1)(\rho^{3m+3}-1)}{(\rho^{m+1}-1)(\rho^{3m+4}-1)} . \qquad (6)$$

For the mode $\pi_{3m+2,3}$

$$\frac{(\rho-1)(\rho^{3m+6}-1)}{(\rho^{m+2}-1)(\rho^{3m+5}-1)} < \frac{a}{D} < \frac{(\rho-1)(\rho^{3m+6}-1)+(\rho-1)^2(\rho^{m+2}-1)}{(\rho^{m+2}-1)(\rho^{3m+5}-1)} . \qquad (7)$$

For the mode $\pi_{4m+1,4}$

$$\frac{\rho(\rho-1)(\rho^{4m+4}-1)}{(\rho^{m+1}-1)(\rho^{4m+5}-1)}-\frac{(\rho-1)^2}{\rho^{4m+5}-1} < \frac{a}{D} < \frac{\rho(\rho-1)(\rho^{4m+4}-1)}{(\rho^{m+1}-1)(\rho^{4m+5}-1)} . \qquad (8)$$

For the mode $\pi_{4m+2,4}$

$$\frac{\rho(\rho-1)(\rho^{m+1}+1)}{\rho^{2m+3}-1}-\frac{(\rho-1)^2}{\rho^{4m+6}-1} < \frac{a}{D} < \frac{\rho(\rho-1)(\rho^{m+1}+1)}{\rho^{2m+3}-1} , \qquad (9)$$
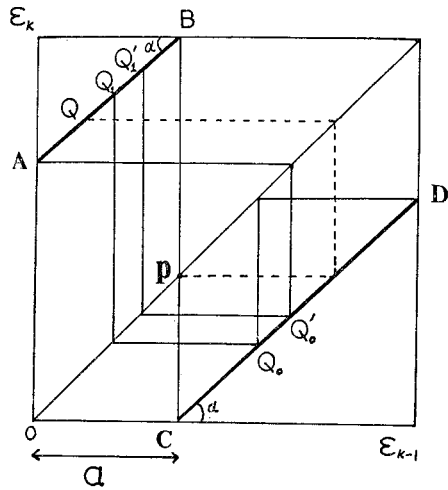
$$\frac{(\rho-1)\,(\rho^{m+2}+1)\,(\rho^{2m+3}+1)}{\rho^{4m+6}-1} < \frac{a}{D} < \frac{(\rho-1)\,(\rho^{m+2}+1)\,(\rho^{2m+3}+1)+(\rho-1)^2}{\rho^{4m+6}-1}\,.$$

$$(10)$$

For the mode $\pi_{4m+3,\,4}$

$$\frac{(\rho-1)\,(\rho^{4m+8}-1)}{(\rho^{m+2}-1)\,(\rho^{4m+7}-1)} < \frac{a}{D} < \frac{(\rho-1)\,(\rho^{4m+8}-1)+(\rho-1)^2\,(\rho^{m+2}-1)}{(\rho^{m+2}-1)\,(\rho^{4m+7}-1)}\,. \qquad (11)$$

It is clear that the width of every band listed above becomes vanishing when $\rho\rightarrow 1$. In Fig. 7 the positions of the cascades of bands, each having vanishing band width, are shown schematically for the case $m=1$ in the space of the control parameter a. It is clear that the distribution of periodic bands is dense across the whole interval, although the width of each band is vanishing.
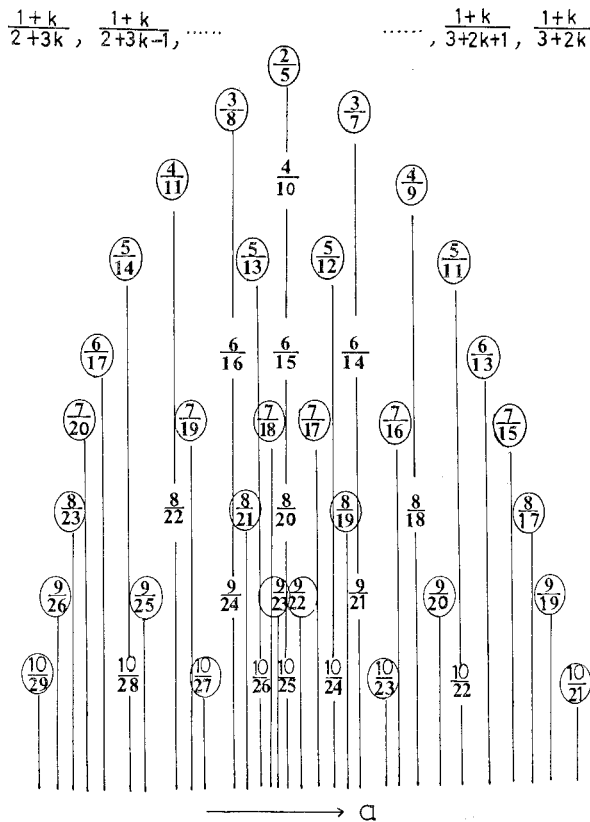

Fig. 7. Locations of periodic modes in a space when $\rho=1$ (the case $m=1$ is indicated). Note that the location q/p corresponds to the periodic mode $\pi_{p-q,q}(n,\,n+1)$. By an appropriate choice of the integer k the sequence of fractions indicated above may be identified with that on a particular level below. In the limit $k\rightarrow\infty$, it is obvious that the set of these numbers is equivalent to that of the rational number.
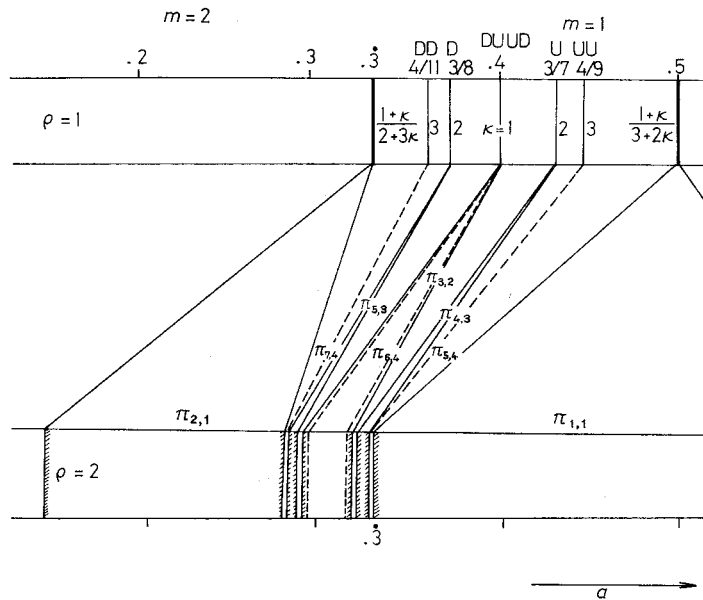
K. Tomita and I. Tsuda

Fig. 8. Locations of periodic bands for typical modes. The case $\rho=2$
is related to the case $\rho=1$.

In Fig. 8 the case $\rho=2$ is shown in contrast to the case $\rho=1$. The main difference lies in that for $\rho=2$ the bands corresponding to relatively short periods dominate the total interval. On the other hand, for $\rho\gtrsim1$ the bands corresponding to very long periods have much more weights than those having shorter periods. It is our contention that the latter situation is directly connected with the possibility of observing chaos in practice.

First of all the long period motions themselves may easily appear as chaotic wanderings. The second and more realistic possibility of chaos arises from a deviation of the transfer function from the assumed linearity in the close neighbourhood of the saddle. This may lead to the change in stability, i.e., the weakly stable orbits are easily destabilized by an introduction of small region in which ρ is less than unity.

Suppose $\rho>1$ except in the δ neighbourhood of the saddle, i.e. $a-\delta<\varepsilon<a+\delta$, and in this interval $\rho'<1$, then the Liapounov number*) $\varLambda$ can be approximately given by

$$\varLambda=2\delta\left(\ln\frac{\rho}{\rho'}\right)-\ln\rho ,\qquad(12)$$

where the total interval is scaled as unity. The orbit under consideration is destabilized when

---

*) For the definition and use of the Lyapounov number see, e.g. G. Benettin, L. Galgani and J. Strelcyn, Phys. Rev. **A14** (1976), 2338.

$$2\delta > \frac{\ln \rho}{\ln \rho - \ln \rho'}. \tag{13}$$

This means that for sufficiently small $(\rho - 1)$ only a small modification is necessary in the close neighbourhood of the saddle for a chaotic wandering to appear. In Fig. 9 an example is shown for this kind of destabilization for the case $\rho = 20/19$ and $\rho' = 10/19$. The condition (13) in this case is well satisfied by $\delta = 0.04$. Figures 9(a) and (b) represent the power spectral densities for $\delta = 0$, which correspond to the periodic motions with period $3(a = 0.33)$ and $60(a = 0.4)$. In Figs. 9(c) and (d) the corresponding power spectral densities are shown for $\rho' = 10/19$ and
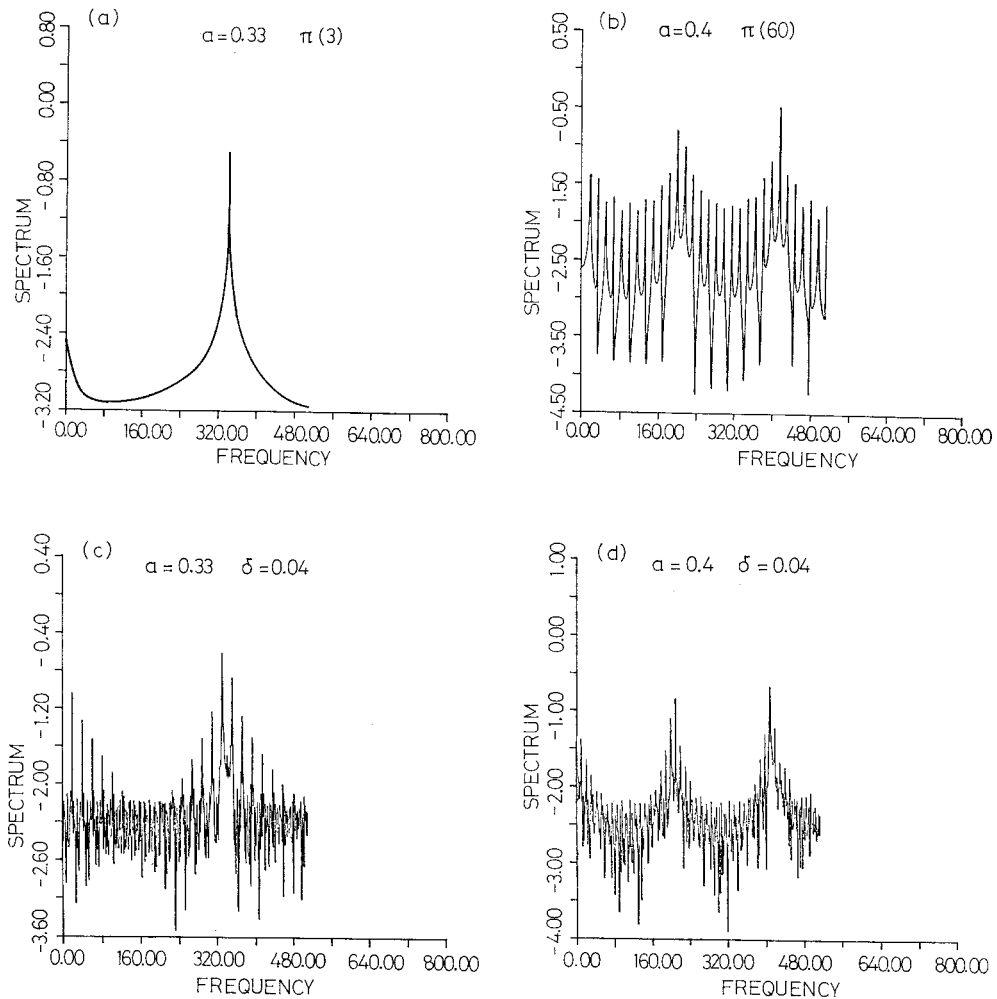
Fig. 9. The power spectra (log scale)—piece-wise linear model.
(a) $a=0.33$, $\delta=0$, (b) $a=0.4$, $\delta=0$, (c) $a=0.33$, $\delta=0.04$, (d) $a=0.4$, $\delta=0.04$.

$\delta = 0.04$. It is obvious that with this slight modification of the transfer function in the neighbourhood of the saddle the orbital stability in (a) and (b) is lost and the original periodic motion acquires a modification of a definitely chaotic character. It is suggested that this kind of deviation from the stable linearity appears in the neighbourhood of the separatrix in Hudson's experiment. In fact when we look at the chaotic switching between 3 and 4 peak modes the last dip in the 4 peak mode decreases when one approaches the separatrix, beyond which the switching to 3 peak mode occurs. This indicates the restriction of orbital excursion in the neighbourhood of the repelling separatrix, which leads to the decrease in the radius of orbital revolution in the upper basin. On the other hand, the area swept by one cycle is expected more or less constant irrespective of the local deformation of the orbit. The fact that the last dip is by far the deepest seems to support this idea, because the last orbit comes close to the saddle and gets through a region in which the angular velocity is very small. This means that in the case of the critical orbits which get over the separatrix during one cycle the orbital radius is increased when it goes beyond the separatrix to the extent that it is decreased before the separatrix. It follows then that the slope of the transfer function in the neighbourhood of the steep step is greater than the average and may lead to the orbital instability in this region, which in turn may easily lead to a positive Liapounov number as is discussed above. This is exactly the situation, supposed before, in which a chaotic switching is expected, and the three chaotic bands $\chi(2, 3)$, $\chi(3, 4)$ and $\chi(4, 5)$ observed in the experiment are considered to arise from this mechanism.

The only exception is the periodic band $\pi_{1,1}(1, 2)$. The most natural explanation is a relatively large value of ρ corresponding to this region. According to the observation of the case $\rho = 2$ compared with $\rho = 1$, it is expected that the relative weight of the periodic bands is much greater than the delocalized orbits even under the local modification of transfer function in the neighbourhood of the saddle.

Case II: $\alpha \gg \beta$

In this case there will be more than one peaks of ϕ_1 inside the relevant interval of ϕ_2, and correspondingly more than one fixed points are expected. None of them, however, are stable at least in the piece-wise linear mapping. There may appear switchings between non-neighbouring $\pi(n)$-like modes as well as nighbouring, but none of them are persisting. It follows then that the asymptotic situation is a practically chaotic switching between several modes, and the whole interval appears mixing. However, there seems to be no indication of this case in Hudson's experiment.

§ 3. Simulation based on the Lorenz plot of the experimental data

In the foregoing section an interpretation of the experimental results due to Hudson et al.[1] has been presented on the basis of a general qualitative considera-

tion of the communication of two basins across a saddle in three dimensional space. It is obvious that at least two dimensional phase portrait is necessary in order to identify the mechanisms proposed. Unfortunately, however, Hudson's observation yields only one variable as a function of time.

In this section, therefore, a one dimensional description of the empirical results is attempted using one dimensional return maps which are obtainable from the observed data. Namely, a transfer function is extracted by plotting the values of successive minima of $x = [Br^-]$ as a function of that one step before. The parametrization of these maps is almost transverse to that proposed in the previous
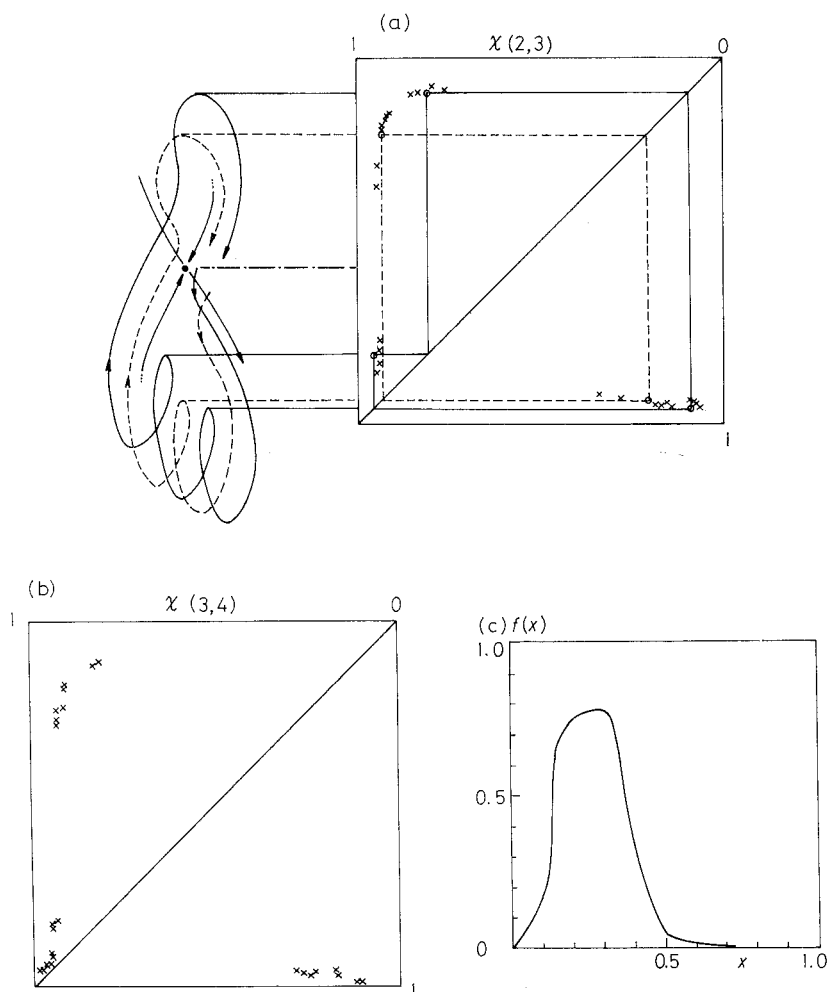

Fig. 10. Empirical Lorenz plot in terms of successive minimum values in Fig. 1.
(a) The case $\chi(2,3)$, (b) the case $\chi(3,4)$, (c) function $f(x)$ given in Eqs. (14.1) and (14.2).

section, however, it is of interest to examine whether the two different parametrizations are compatible with each other.

In Fig. 10 typical examples of the one dimensional Lorenz plot are shown for $\chi(2,3)$ and $\chi(3,4)$ using the successive minimum values of the $[Br^-]$ electrode potential x. It is remarkable that the representative points form a fairly simple single humped function $f(x)$ although there are gaps between islands. The definiteness of this function assures that the seeming chaos is of a deterministic origin, thus the possibility of a noise of external origins is precluded.

It should also be noted that the two Lorenz plots are almost identical in shape, but the plot for $\chi(2,3)$ is shifted slightly upward with respect to that for $\chi(3,4)$. In view of this fact a trial was made to shift the function $f(x)$ obtained above vertically without changing its shape, and see how the mapping behaves asymptotically as a function of the amount of shift b, which in turn is a function of the control parameter.

For this purpose the function $f(x)$ is approximated by an analytic function, which is given by

$$f(x) = \{\pm(\pm x \mp 0.125)^{1/3} + 0.5\}e^{-x}, \quad (0 \leq x < 0.3) \tag{14·1}$$

where the upper and lower signs stand for $0.125 \leq x$ and $x < 0.125$, respectively.

$$f(x) = \frac{B}{A}\frac{10}{\Gamma(20)}\left(\frac{190}{3}x\right)^{19}e^{-(190/3)x}, \quad (0.3 \leq x) \tag{14·2}$$

Table IV. The asymptotic modes expected for the shifted empirical transfer functions (arranged according to the magnitude b of the vertical shift).

b	the character of the asymptotic orbit
0.2	$\pi(2)$
0.12	$\pi_{3,0}(2,3)$
0.115	$\pi_{1,3}(2,3)$
0.1147	$\chi(2,3)$
0.1146	$\pi_{1,4}(2,3)$
0.0515	$\pi(3)$
0.0502	$\pi_{2,0}(3,4)$
0.049	$\chi(3,4)$
0.0488	$\pi_{2,3}(3,4)$
0.04	$\pi(4)$
0.0265	$\pi_{2,0}(4,5)$
0.0263	$\chi(5,4)$
0.0261	$\pi_{2,2}(4,5)$
0.026	$\chi(4,5)$
0.02	$\pi(5)$
0.01	$\pi(13)$

where $A = \{10/\Gamma(20)\}(19)^{19}e^{-19}$, $B = \{(0.175)^{1/3} + 0.5\} e^{-0.3}$, (cf. Fig. 10 (c)) and $\Gamma(x)$ is the gamma function. As a shifted transfer function $F(x) = f(x) + b$ is adopted and the asymptotic behaviour of the new mapping is investigated for various fixed values of b. In Table IV the results are summarized using the notations defined in §1.

The contents of Table IV are established by inspecting the time sequence and the frequency spectra shown in Fig. 11. The chaotic phases are unambiguously
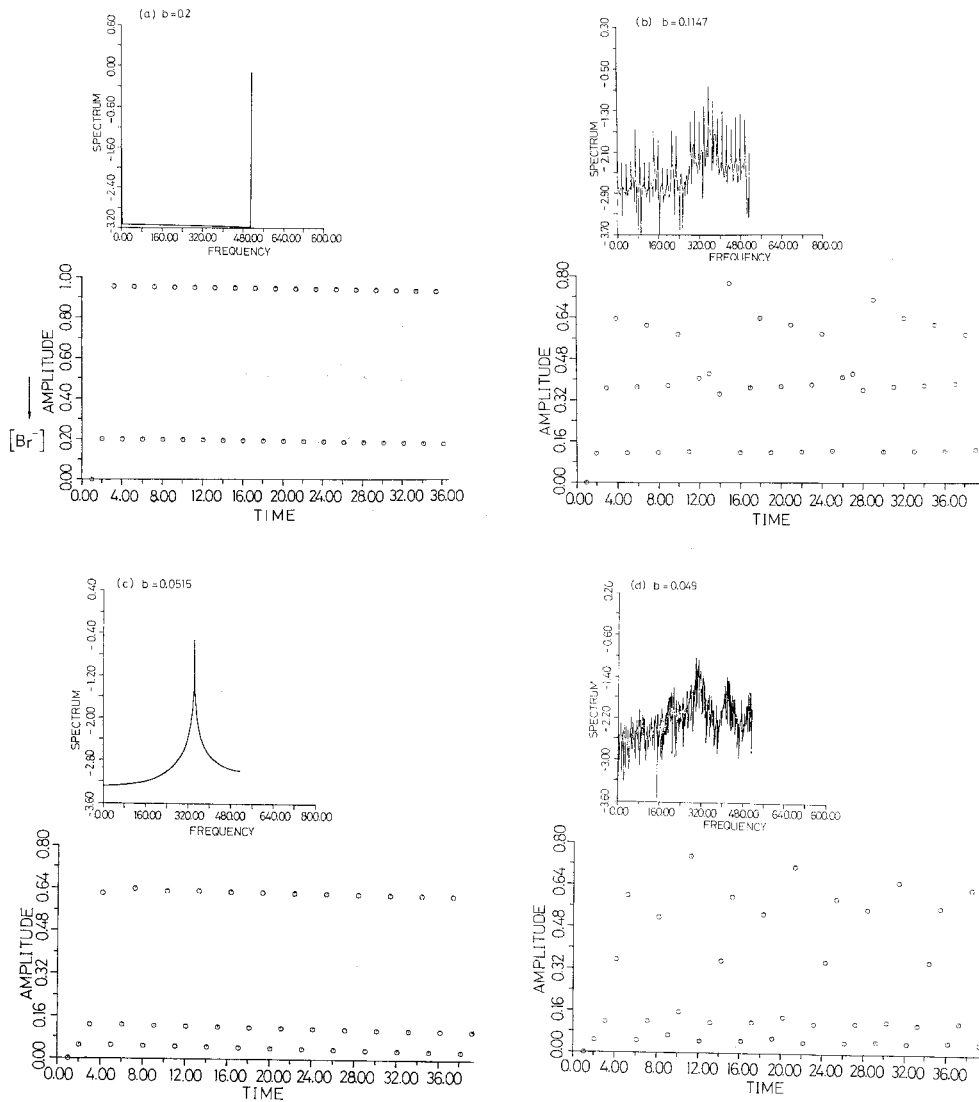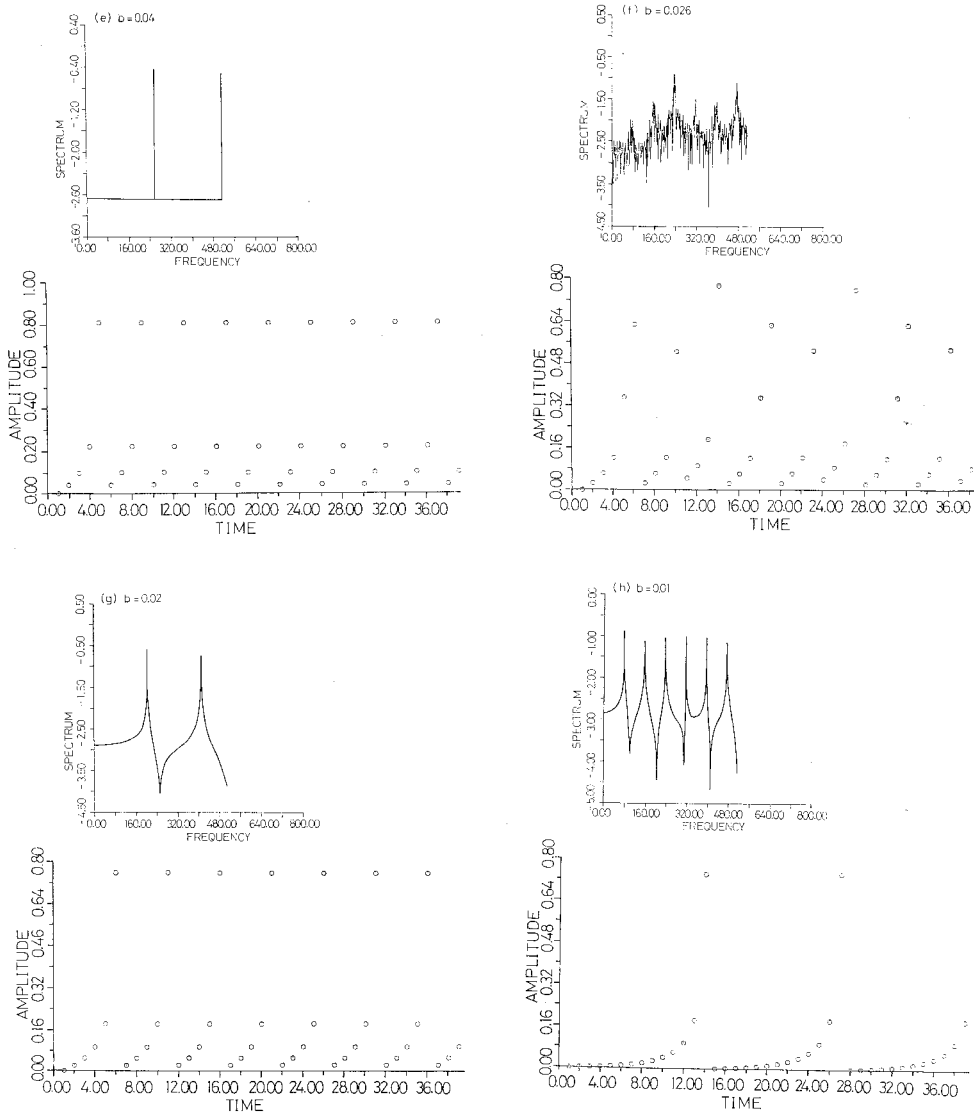

Fig. 11. (Continued)

Fig. 11. The power spectra (log scale)—shifted empirical transfer function.
(a) $\pi(2)$, (b) $\chi(2,3)$, (c) $\pi(3)$, (d) $\chi(3,4)$, (e) $\pi(4)$, (f) $\chi(4,5)$, (g) $\pi(5)$,
(h) $\pi(13)$. In each case the lower figure indicates the successive minimum
values of [Br$^-$] as a function of time.

recognized by the existence of a continuous component in the frequency spectrum.[*]

---

[*] The sharp frequency peak which represents the periodic mode is often accompanied by a slowly varying continuous background apart from the white noise which is always present. This, however, is not an indication of an intrinsic chaos, but a result due to extrinsic origin. Namely, a purely periodic mode may acquire this kind of continuous background simply because the length of period does not commensurate with the adopted sampling which is characterized by 2^n.
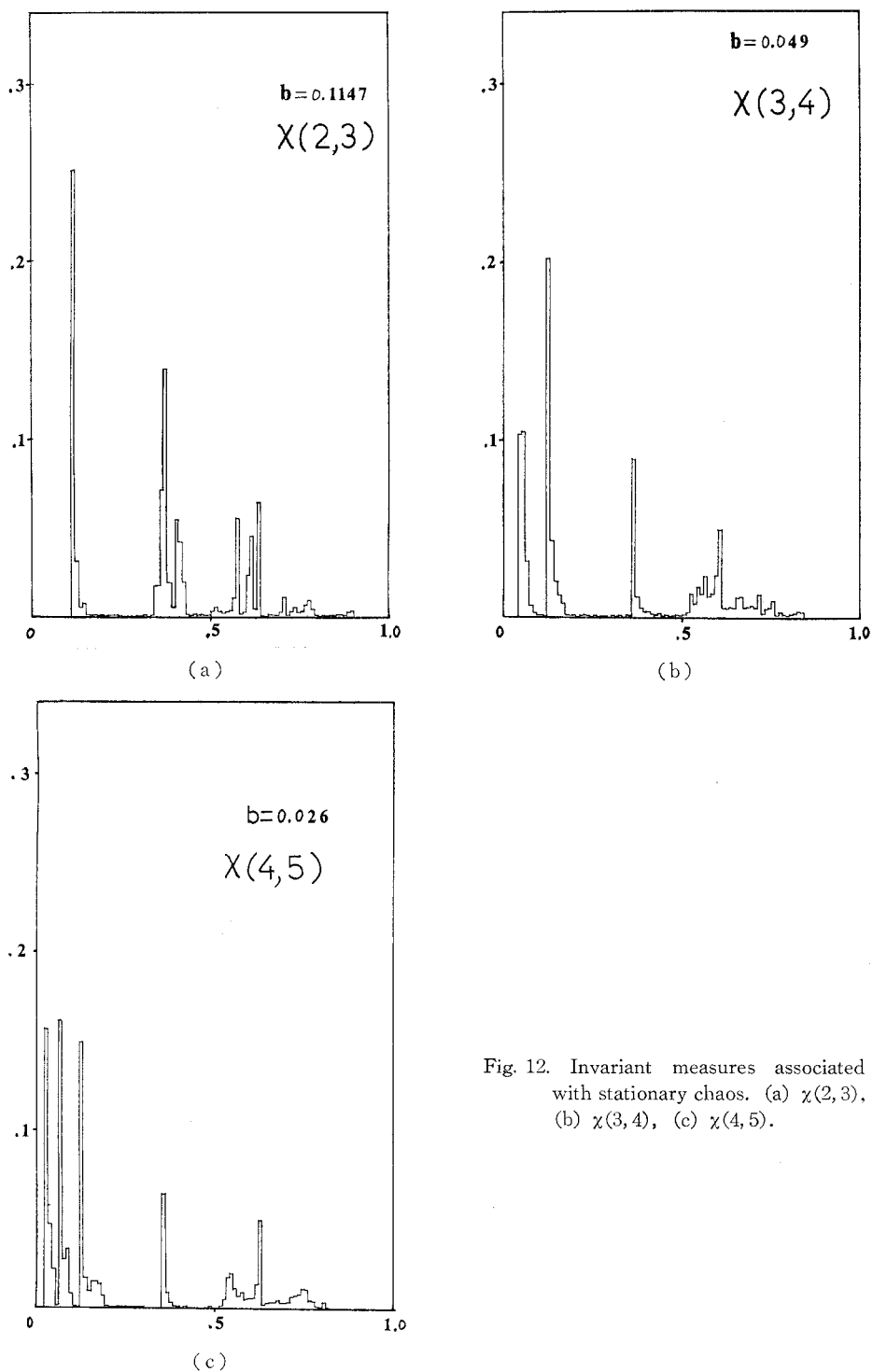
Fig. 12. Invariant measures associated with stationary chaos. (a) $\chi(2,3)$, (b) $\chi(3,4)$, (c) $\chi(4,5)$.

In Fig. 12 the empirical invariant measures defined by

$$\rho(x) = \lim_{n \to \infty} \frac{1}{n} \sum_{i=0}^{n-1} \delta\left(x - F^{(i)}(x_0)\right) \tag{15}$$

are plotted for the chaotic phases $\chi(2, 3)$, $\chi(3, 4)$ and $\chi(4, 5)$, which are consistent with the observed data (Figs. 10(a), (b)) in their structure.

The similarity between the sequence in Table IV to that in Table I is clear, although the relation between b and the rate of flow may only be established a posteriori. It is perhaps more remarkable that the sequence common to both tables are essentially identical with the sequence predicted by a simple piecewise linear model introduced in §2. This is considered as an evidence that the idea of chaos due to incommensurate delocalization ruled by the intervening saddle is essentially correct.

The existence of practically diverging slope in Fig. 10 clearly corresponds to the existence of a separatrix due to the saddle. The increase in b in $F(x)$ results in the leftward shift of this point as well as the maximum point of $F(x)$ in the asymptotic square frame. The left-hand extreme of $F(x)$ in the square is enhanced accordingly, which is an indication that one is coming closer to the separatrix. The situation is exactly similar to that in §2 when the asymptotic square is shifted toward the right direction with respect to the saw-tooth. The position of the step due to the saw-tooth corresponds to the position of a saddle of which the existence is presupposed.

In Fig. 10(a) the Lorenz plot is associated with a plausible orbital phase portrait in two-dimensional projection. It should be noted that this orbital phase portrait is essentially identical with that introduced in §2 with reference to the piecewise linear model for the Lorenz plot, although the two chosen directions for the Lorenz plot are almost transverse to each other.

In Table IV the maximum value in b for a chaotic behaviour is found to be 0.1147. This value is shown to be consistent with the condition $b < \tilde{b} = 0.1196$ for the existence of a chaotic orbit with respect to $F^{(1)}$ obtained by the snap-back argument.[4] The equal sign corresponds to the situation specified by $a = \tilde{a}_1$ in the logistic model,[5] i.e., the limit of mixing in a single domain. The region $b < \tilde{b}$ in the former corresponds to the region $a > \tilde{a}_1$ in the latter.

§4. Summary and discussion

In summary the possible emergence of a chaotic behaviour due to incommensurate delocalization is demonstrated by introducing a one dimensional Poincaré return map with a simple behaviour. It is admitted that the piecewise linear approximation may not be enough for a quantitative description; however, the observed characteristics of the Belousov-Zhabotinsky reaction as a function of the control parameter, namely the appearance of a cascade of periodic phases and a

chaotic behaviour between two consecutive periodic phases, are well understood by this model at least qualitatively.

The gist extracted from the simple model is that according to a moderate change in the control parameter the transfer function in the Lorenz plot is essentially shifted without an appreciable change in its shape. This idea, when applied to the observed data, yields a remarkably similar sequence of phases to those found experimentally and also to those expected by the simple model.

Although the mechanism for the onset of a single chaos has been discussed in various ways, little attempt is known to allocate various phases (i.e., plural number of periodic and chaotic phases) on the phase diagram in a systematic way. In this context it should perhaps be emphasized that the overall structure in the control parameter space has been discussed here by using a single model.

The following properties have been required for the simple model. Let us recapitulate them here together with some discussions of the physical background:

1) Two branches (i.e., the flowless bulk branch and the flow-induced branch) are delocalized across an intervening saddle.

This means that each of the two branches may physically be realized under some condition and there appear essentially three steady states under the condition under consideration.

2) The Poincaré return maps form an approximately one-dimensional section, which may be parametrized by a single parameter (i.e., ε_k).

This means that a single positive eigenvalue characterizes the invariant manifold.

3) The transfer function in the Lorenz plot is monotone increasing, and is weakly contracting (i.e., $\rho \equiv d\varepsilon_{k-1}/d\varepsilon_k \gtrsim 1$) except in the neighbourhood of the saddle.

This means that outside the range of strong repulsion due to the separatrices the phase space is fairly homogeneous and translationally invariant. The weak contraction of the map is considered to originate from the global stability.

4) When the angular drift ε_k reaches a value corresponding to a whole cycle in the upper basin, the number of cycle is reduced by one and the ε_k is reduced to zero from which it resumes to increase.

This means that the transfer function is of shift type (i.e., saw-tooth type).

5) In the close neighbourhood of the saddle (i.e., the steep step in the transfer function) there appears an expanding map which leads easily to the destabilization of the entire orbit (i.e., chaos).

This could be understood if one is ready to anticipate the following behaviours of the orbit.

(a) The separation of orbits is decreased in the part of the cycle before the separatrix due to the influence of its repulsion.

(b) On the other hand, it is increased in the part of the cycle beyond the separatrix, so that the area swept by a whole cycle tends to be conserved. It is this

increase in the separation of orbits that leads to the expanding nature of the map in the neighbourhood of the saddle (i.e., the steep step).

6)   The dependence on the control parameter appears through the saddle angle θ or the available homogeneous angular domain for the cycles in the upper basin.

Increase in the available domain implies the increase in the number of cycles before it goes beyond the separatrix, thus the saddle angle should increase with increasing rate of flow.

Coming back to the experimental data the following comments may be due at this stage.   First, the fact that the invariant manifold is two-dimensional in a good approximation implies that a three dimensional model would be enough to describe the qualitative behaviour.   Secondly, it is not difficult to understand that change either in temperature or in the total concentration of Ce leads to similar structure of phases in the parameter space.   Increase either in temperature or the total celium concentration is expected to lead to the increase in the rate of reaction. This means that it leads to a result similar to the case in which the rate of flow is decreased under constant temperature or total celium concentration.   The observed characteristics are certainly consonant with this kind of tendency.   Finally, in the realistic case the bifurcation characteristics may be different from the simple model indicated in Fig. 2, including the possibility of inverted bifurcations.

In Hudson's experiment $\pi(n)$ is identified only up to $n=5$, and one data beyond this appears $\pi(n:\text{ large})$ with very small initial radius.   This kind of behaviour may be expected if the available part of the upper basin and consequently the orbital radius are rapidly decreasing in this range of control parameter.   Suppose the radius becomes so small that the orbit is practically confined to the region under the influence of the local separatrix, it is easy to expect a quasi-periodic motion and even a single small limit cycle confined in the upper basin to appear instead of $\pi(\infty)$.   This seems to correspond to the final situation in Hudson's data which indicate a doubly periodic motion and then a flow-induced limit cycle.

A similar simple theoretical consideration may apply to a symmetric two basins intervened by a saddle, as in the case of the Lorenz model.[6]   In this case the cascade of periodic phase alternates in the symmetry of orbits with respect to the intervening saddle.   Apart from this property the appearance of intercalated chaos is quite similar to the case discussed above.   The details will be reported in a separate publication.

Appendix

An economical method is described in this appendix for finding a condition under which the image of the gap (Q_0, Q_0') in Fig. 6 overrides the saddle for the first time at the n-th mapping.   The idea is based on the recognition that there

exists a systematic sequence of mapping in the course of which the non-overriding property of the gap is inherited. Namely, when the image of the gap on AB does not override the inverse image Q of the fixed point P, representing the saddle, there will never appear overriding before it comes back onto AB for the next time. This observation enables us to confine our attention to the branch AB only.

Suppose that the first image of the gap (Q_0, Q_0') on AB is given by (Q_1, Q_1'), then the condition may be obtained for this interval to include the first inverse image Q of the fixed point P in terms of the abscissa $a (\equiv OC)$ of P and the factor $\rho (\equiv 1/\tan \alpha)$ representing the contraction of the mapping. Suppose $2a < D$ and the point Q is reached from P after $(m+1)$ steps of inverse mapping by CD, then the required condition may be shown to be

$$\frac{(\rho-1)(\rho^{m+2}+1)}{\rho^{2m+3}-1} < \frac{a}{D} < \frac{\rho(\rho-1)(\rho^{m+1}+1)}{\rho^{2m+3}-1} . \tag{A$\cdot$1}$$

It is straightforward to examine that the resulting periodic orbit consists of $2m+3$ fixed points, of which 2 belongs to the branch AB, corresponding to $\pi(n+1)$, and $2m+1$ belongs to the branch CD, corresponding to $\pi(n)$. Therefore, the resulting orbit may be denoted by $\pi_{2m+1,2}(n, n+1)$ in the notation defined in § 1. For the special case $\rho=1$, the relevant band (A$\cdot$1) is placed at $2/(2m+3)$ and with vanishing width.

When the interval (Q_1, Q_1') does not include the point Q, two cases should be distinguished according to the side on which the interval (Q_1, Q_1') off-shoots the point Q. When it undershoots Q, the image (Q_2, Q_2') of (Q_1, Q_1') on AB in the next round is bound to climb up along AB, and the condition for this second image (Q_2, Q_2') to override Q is given by

$$\frac{\rho(\rho-1)(\rho^{3m+3}-1)-(\rho-1)^2(\rho^{m+1}-1)}{(\rho^{m+1}-1)(\rho^{3m+4}-1)} < \frac{a}{D} < \frac{\rho(\rho-1)(\rho^{3m+3}-1)}{(\rho^{m+1}-1)(\rho^{3m+4}-1)} . \tag{A$\cdot$2}$$

The resulting periodic orbit is represented by $3m+4$ fixed points, of which 3 belongs to the branch $\pi(n+1)$ (AB) and $3m+1$ belongs to the branch $\pi(n)$ (CD). Therefore, it may be denoted by $\pi_{3m+1,3}(n, n+1)$. For the special case $\rho=1$ the relevant band (A$\cdot$2) is placed at $3/3m+4$ and with vanishing width.

When (Q_1, Q_1') overshoots Q, then the image (Q_2, Q_2') of (Q_1, Q_1') in the next round on AB is bound to come down along AB, and the condition for (Q_2, Q_2') to override Q is given by

$$\frac{(\rho-1)(\rho^{3m+6}-1)}{(\rho^{m+2}-1)(\rho^{3m+5}-1)} < \frac{a}{D} < \frac{(\rho-1)(\rho^{3m+6}-1)+(\rho-1)^2(\rho^{m+2}-1)}{(\rho^{m+2}-1)(\rho^{3m+5}-1)} . \tag{A$\cdot$3}$$

The resulting periodic orbit is represented by $3m+5$ fixed points, of which $3m+2$ belong to the branch $\pi(n)$ (CD) and 3 belong to the branch $\pi(n+1)$ (AB). Therefore it is denoted by $\pi_{3m+2,3}(n, n+1)$. For the special case $\rho=1$

the band (A·3) is placed at $3/3m+5$ with vanishing width.

Repeating similar procedures the bands corresponding to higher order overridings are obtained, which are shown in Fig. 7.

References

1) J. L. Hudson, M. Hart and D. Marinko, J. Chem. Phys. **71** (1979), 1601.
2) K. Tomita and I. Tsuda, Phys. Letters **71A** (1979), 489.
3) C. Murakami and K. Tomita, J. Theor. Biol. **79** (1979), 203.
4) F. R. Marotto, Comm. Math. Phys. **68** (1979), 187, and references 5 and 7 cited therein.
5) S. Grossmann and S. Thomae, Z. Naturforsch. **32a** (1977), 1353.
6) E. N. Lorenz, J. Atmos. Sci. **20** (1963), 130.
7) J. L. Hudson (private communication).